Medical Engineering and Physics 110 (2022) 103919

Contents lists available at ScienceDirect

Medical Engineering and Physics

journal homepage: www.elsevier.com/locate/medengphy

Shannon entropy as a reliable score to diagnose human fibroelastic degenerative mitral chords: A micro-ct ex-vivo study

Diego Ferreño [a,*], José M. Revuelta [a,b], José A. Sainz-Aja [a], Carlos Wert-Carvajal [c,d], José A. Casado [a], Soraya Diego [a], Isidro A. Carrascal [a], Jacobo Silva [e], Federico Gutiérrez-Solana [a]

[a] LADICIM (Laboratory of Materials Science and Engineering), University of Cantabria. E.T.S. de Ingenieros de Caminos, Canales y Puertos, Av/Los Castros 44, 39005 Santander, Spain
[b] Cardiovascular Surgery. Hospital Universitario Marqués de Valdecilla, Av/Valdecilla, s/n, 39008 Santander, Spain
[c] Universidad Carlos III de Madrid. Avda. de la Universidad, 30. 28911 Madrid, Spain
[d] University of California, San Diego. 9500 Gilman Drive, MC 0412 La Jolla, California
[e] Hospital Universitario Central de Asturias, Av. Roma, s/n, 33011 Oviedo, Asturias, Spain

ARTICLE INFO

Keywords:
Mitral chordae tendineae
Degenerative mitral valve disease
Micro computerized tomography
Shannon entropy
K-means
Machine learning

ABSTRACT

This paper is aimed at identifying by means of micro-CT the microstructural differences between normal and degenerative mitral marginal chordae tendineae. The control group is composed of 21 normal chords excised from 14 normal mitral valves from heart transplant recipients. The experimental group comprises 22 degenerative fibroelastic chords obtained at surgery from 11 pathological valves after mitral repair or replacement. In the control group the superficial endothelial cells and spongiosa layer remained intact, covering the wavy core collagen. In contrast, in the experimental group the collagen fibers were arranged as straightened thick bundles in a parallel configuration. 100 cross-sections were examined by micro-CT from each chord. Each image was randomized through the K-means machine learning algorithm and then, the global and local Shannon entropies were obtained. The optimum number of clusters, K, was estimated to maximize the differences between normal and degenerative chords in global and local Shannon entropy; the p-value after a nested ANOVA test was chosen as the parameter to be minimized. Optimum results were obtained with global Shannon entropy and $2 \leq K \leq 7$, providing $p < 0.01$; for K=3, $p = 2.86 \cdot 10^{-3}$. These findings open the door to novel perioperative diagnostic methods in order to avoid or reduce postoperative mitral valve regurgitation recurrences.

1. Introduction

Over the last two decades, the prevalence of mitral valve regurgitation (MVR) has increased along with the longevity of the general population; in particular, the degenerative regurgitation which affects about 2% of the population [1,2]. The functional competence of the mitral valve [3–5] depends on the coordinated interaction between its components. Different pathologies can affect the geometry, structure or intrinsic properties of the valve mechanism, resulting in MVR. According to the Carpentier classification [6,7], the mitral valves with elongated or ruptured chordae tendineae are classified as type II valves, where the increased abnormal motion produces the leaflet prolapse or a floppy valve.

Recurrence of regurgitation is not a rare postoperative complication after mitral reconstructive surgery, with a reported linearized incidence of 3.7% to 8.3% per year. Only half of patients remain free from postoperative mitral insufficiency at mid-term follow-up [8] after valve repair. Reoperation rate after repair increased with time (7% at 5 years, 11% at 10 years, 16% at 15 years, and 20% at 19.5 years) [9].

The most frequent degenerative mitral regurgitation [10] is fibroelastic deficiency which mainly affects patients over 60 years. Fibroelastic deficiency refers to a spectrum of degenerative valve diseases in which morphologic changes in the connective tissue of the mitral valve cause significant structural lesions that prevent normal function of the mitral apparatus, in most cases requiring repair by experienced surgeons [11,12]. In a previous study [13], we found by light and ultrastructural microscopic analyses that both the extracellular matrix and the interstitial cells are severely affected in the degenerative disease.

* Corresponding author at: LADICIM (Laboratory of Materials Science and Engineering), University of Cantabria. E.T.S. de Ingenieros de Caminos, Canales y Puertos, Av/Los Castros 44, 39005 Santander, Spain.
E-mail address: ferrenod@unican.es (D. Ferreño).

https://doi.org/10.1016/j.medengphy.2022.103919
Received 14 March 2022; Received in revised form 12 September 2022; Accepted 3 November 2022
Available online 8 November 2022

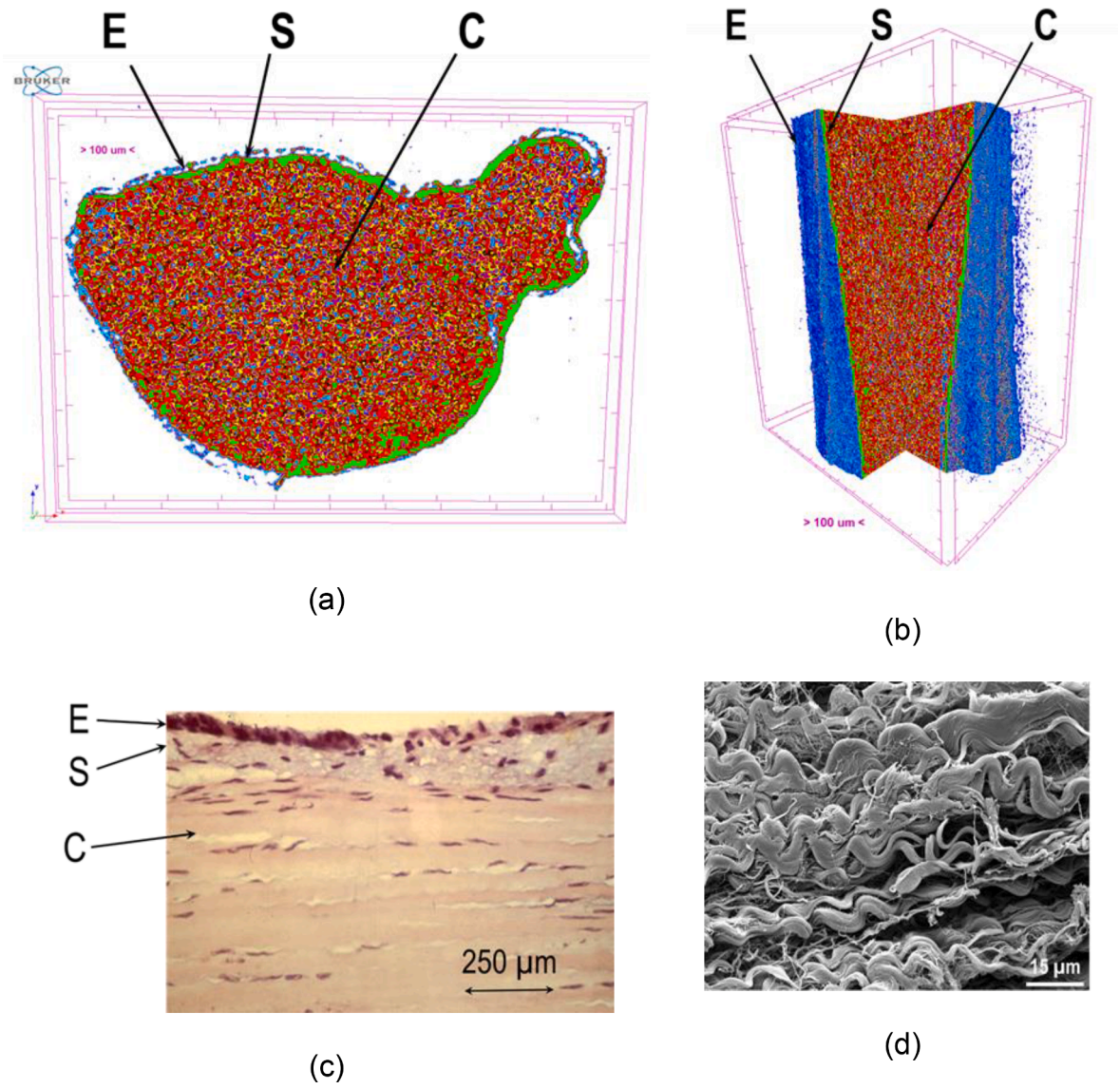

Fig. 1. (a) Micro-CT cross-section of a normal marginal chord from a heart transplant recipient. The external layers of endothelial (E) cells (blue) and the spongiosa (S) layer (green) surround the dense core (C) composed of collagen fibers. (b) Longitudinal section of the same chord. (c) Light microscopy of a longitudinal section of a normal human MCT. (d) SEM micrograph showing the core collagen fibers of a normal MCT arranged in a wavy configuration.

Mitral chordae tendineae (MCT) must show an elastic and resistant response to withstand the repetitive forces of the cardiac cycle. Crimped collagen fibers, elastin fibers and the outer layer of endothelial cells are the main structural components for the mechanical function of MCT [14, 15]. The microstructure of normal and degenerative human MCT was determined in this study by means of micro X-ray computed tomography (micro-CT). The microstructural characterization of MCT was addressed in several previous contributions [16–18] using light and Scanning Electron Microscopy (SEM); to the best of the authors' knowledge, this is the first study where micro-CT has been used to determine the microstructure of the MCT.

The main advantage of micro-CT is that it enables the chordal examination without altering their delicate integrity and, therefore, it eliminates the possible artefacts due to the preparation of samples by conventional methods. The microstructural features of the diseased chordae were identified and compared to those of normal MCT. A completely automatic procedure was implemented, which combines the use of the K-means unsupervised clustering algorithm with the Shannon entropy (SE) concept [19]. The global and local Shannon entropies (GSE and LSE, respectively) were employed. The number of clusters in K-means, K, was estimated through an iterative procedure to maximize the differences between normal and degenerative chords. The statistical significance of the differences was assessed through a Nested ANOVA test.

This research was developed under the approval of the Ethics Committee of the Marqués de Valdecilla University Hospital (Santander, Spain), in agreement with the World Medical Association Declaration of Helsinki (Ethical Principles for Medical Research Involving Human Subjects).

2. Methods

2.1. Available material

43 human marginal MCT specimens were obtained at surgery and transported to the laboratory LADICIM of the University of Cantabria in a portable refrigerator at 4°C. Mitral valve specimens were categorized into two groups of MCT: (a) 21 normal chords were excised from 14 normal mitral valves from heart transplant recipients without valve pathologies (8 males, 6 females; mean-aged 59 ± 8 years, range: 36 – 72

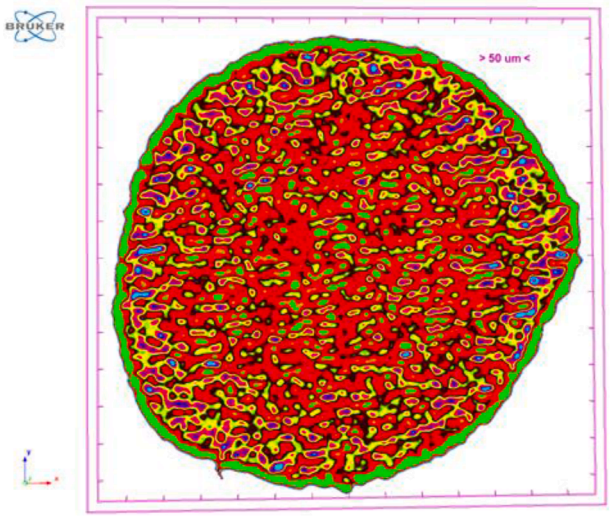

(a)

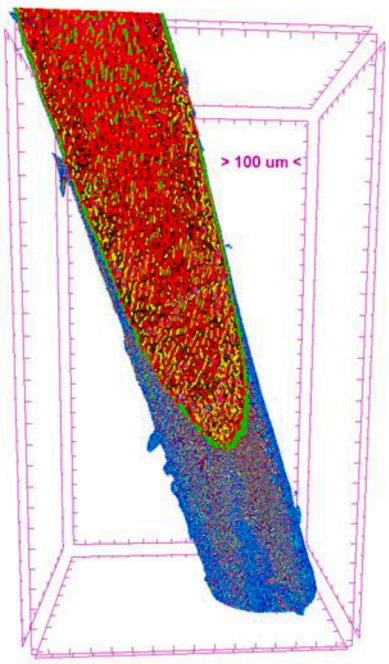

(b)

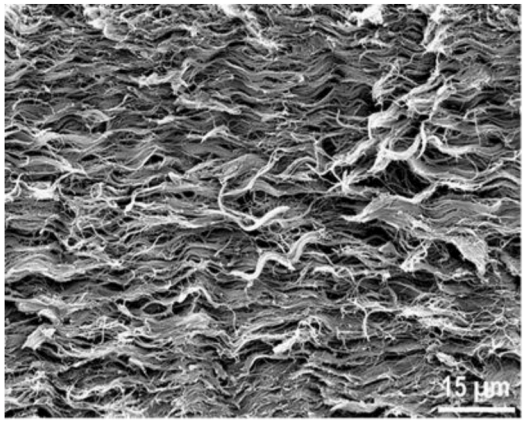

(c)

Fig. 2. (a) Micro-CT cross-section view of a degenerative marginal chord. (b) Longitudinal cross-section of the same chord. (c) SEM micrograph of a degenerative marginal chord. Collagen bundles of the core have lost their wavy appearance.

years) (Group I). (b) 22 degenerative chords obtained at surgery from 11 fibroelastic degenerative valves (5 males, 6 females; mean-aged 66 ± 7 years, range: 56 – 78 years), after mitral repair or replacement (Group II). Heart transplant recipients with normal mitral valves at preoperative echocardiographic study were selected after a careful surgical inspection as the control group (Group I). Only fresh normal valves were included in this study to avoid the postmortem collagen and fibroelastic tissue deterioration, or abnormal functional MCT.

Following the protocol by Prot et al. [20], the specimens were stored in a freezer (-18 °C) and slowly thawed before testing, to preserve the integrity of the biological material after the surgical excision of the valves. Marginal MCT were removed including a portion of their leaflet insertion and papillary muscle. In the case of MCT with branches, the main strand from the papillary muscle to the leaflet was selected, and the secondary branches were carefully trimmed [21]. Two chords, randomly selected from each group, were examined under optical and scanning electron microscopy while the rest of them were observed by micro-CT.

2.2. *Micro-computed tomography*

Nondestructive microstructural inspection of the MCT was carried out employing a Skyscan 1172™ micro-CT equipped with a 80 kV and 100 µA X-ray source. The image resolution was 2 µm measured through

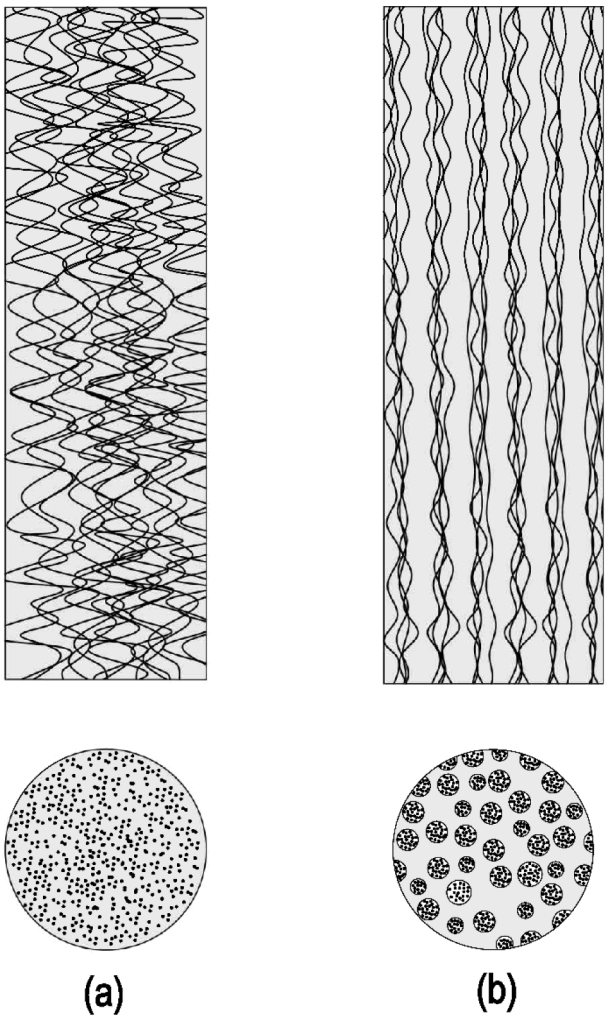

Fig. 3. Schematic description of the structural organization of normal (a) and degenerative (b) chords.

the image pixel size and had an 8-bit color depth. Reconstruction was conducted employing the software NRecon-Bruker™ [22]. The following parameters were used for scanning and reconstruction. Scanning: Source Voltage = 40 kV, source Current = 100 μA, image Pixel Size = 2 μm, exposure time = 0.6 s, rotation step = 0.500 deg. Reconstruction parameters: ring Artifact Correction=6, smoothing=1, beam hardening correction =31 %. The duration of the scanning process was less than 30 minutes to minimize the dehydration of the tissues.

2.3. Image analysis

The central region of each MCT was scanned over a length of 2 mm, obtaining 100 images of cross sections evenly distributed (one section every 20 μm). The processing of micro-CT images to distinguish between normal and degenerative MCT was conducted by means of a completely automated procedure. Image randomness can be measured using a variety of methods [23]. The differences visually observed between normal and degenerative MCT can be expressed in terms of the texture (or randomness) of the images. Texture provides information about the spatial arrangement of the grayscale in an image and can be used as a feature to partition images into regions of interest and to classify those regions [24]. If the texture elements are small and tonal differences between them are large, a fine texture results; on the contrary, if they are large and consist of several pixels, a coarse texture is obtained [24]. The Region of Interest (ROI) for all cross-sectional images was chosen as a centered square of 200 μm of side length [25].

The K-means clustering algorithm was used on each of the 100 cross-section images from each MCT. K-means is widely used in data mining and machine learning for the partition of a number of observations into K clusters so that each observation is assigned to the cluster (Voronoi cell) with the nearest mean [26,27]. In this way, this algorithm can be used for image segmentation, to partition an image into regions each of which has a reasonably homogenous visual appearance. K-means requires the user to provide the number of clusters, K, as an initial hyperparameter [28]. The grayscale histogram of each of the micro-CT images was clustered by K-means using values of K between 2 and 16. Thus, for instance, when K=2, the grayscale histogram was binarized optimizing the two values (between 0 and 255 corresponding to 8-bit images) of the grayscale through the K-means method. Similarly, for K=3 each image was clustered in three values of the grayscale and so on. K-means acts as a scalable vector quantization method, which guarantees texture analysis robustness among images [29]. Next, the normalized histogram of graylevel differences was determined.

Shannon entropy, SE, is a measure of the uncertainty associated with a random variable and has become one of the most widely employed scores for image analysis [30]. The SE of an individual image after the K-means clustering is defined by (1):

$$H_K = -\sum_{i=1}^{i=K} p_i \cdot \ln p_i \quad (1)$$

where 'i' represents each of the density levels for a given number, K, of clusters and p_i is the normalized frequency of that level 'i' in the grayscale histogram. H_K is a measure of the homogeneity of the histogram which is maximised for uniform histograms (the theoretical maximum of the SE score for an image would be ln(256) which occurs when each grayscale is equally likely) [23]. The average entropy of the 100 cross-sections was computed as a measure of the entropy of the chord. This entropic measure of texture will be referred to as global Shannon entropy, GSE. In addition, subsets of the initial ROI (local image blocks [23]) were created with square selections of 2, 3, 9 and 12 pixels of side length, respectively, to determine the local Shannon entropy, LSE, for different numbers of pixels. LSE of each MCT is the average SE of all the subsets in the chord. This estimator serves as a test of independence of the scale and the level of organization. This procedure is adapted from the method devised by Wu et al. [23]. As stated by these authors, LSE is able to overcome some of the limitations of GSE because image randomness is obtained from non-overlapping image blocks; thus, GSE may be inconsistent for images with various sizes; in general, an image of a larger size tends to have a higher GSE score than a smaller size image. Therefore, measuring randomness using GSE is size-dependent whereas LSE minimizes this effect [23]. In addition, the efficiency of LSE is greater because in many cases it requires only a portion of the total pixel information (in the study by Wu et al. [23], only a reduced number of image blocks were selected, rather than the total number of subsets, as in this study). In this research, windows of 2, 3, 9 and 12 pixels were selected because of their low size compared to the actual ROI. LSE serves for validating that differences in structure between degenerative and functional chords do not occur because of the section that is chosen. Thus, degenerative chords are expected to display a higher SE for whichever area inside the ROI has been selected. Finally, after determining GSE and LSE, the optimum number of clusters was obtained. In our approach, K was estimated to maximize the differences between normal and degenerative chords in SE [23].

The relation between K-means and SE comes from the fact that original contrast-levels are sample-dependent and noisy, which renders them as unsuitable for an analysis based on the density distribution. K-means is used as a denoising method and for contrast regularization. In a low-dimensional form, the histogram can only reflect structural information – i.e., the distribution of n elements, which if equal in density maximize SE. Thus, SE becomes a metric of randomness of the image

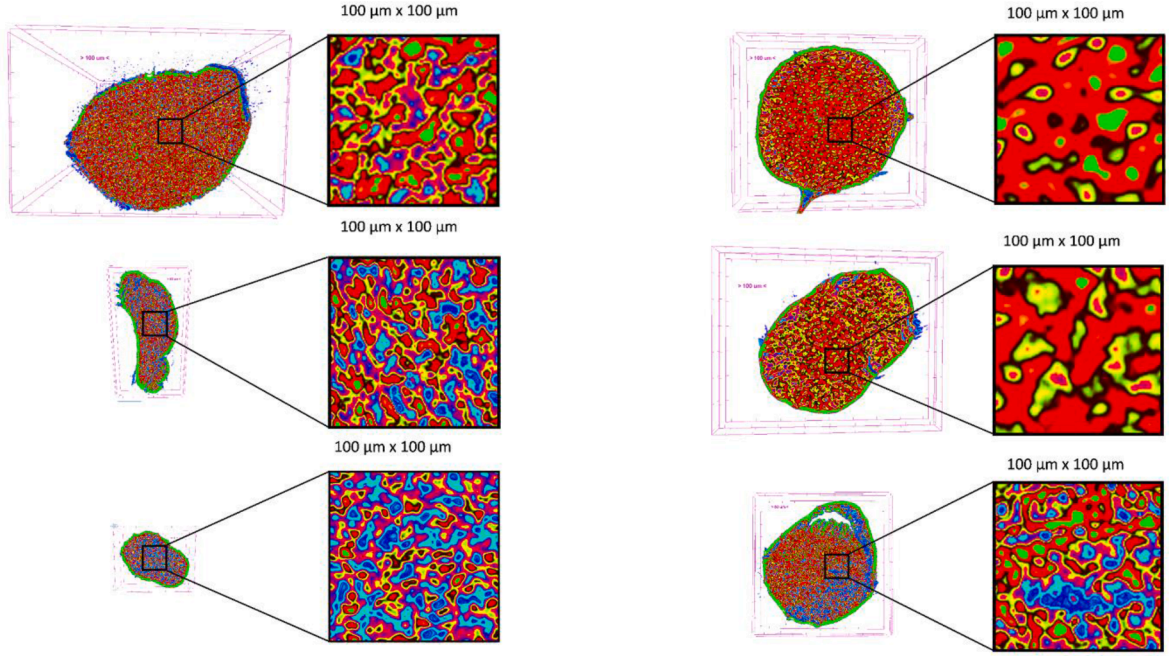

Fig. 4. Panel of micro-CT images comparing the texture of normal (left) and degenerative (right) MCT.

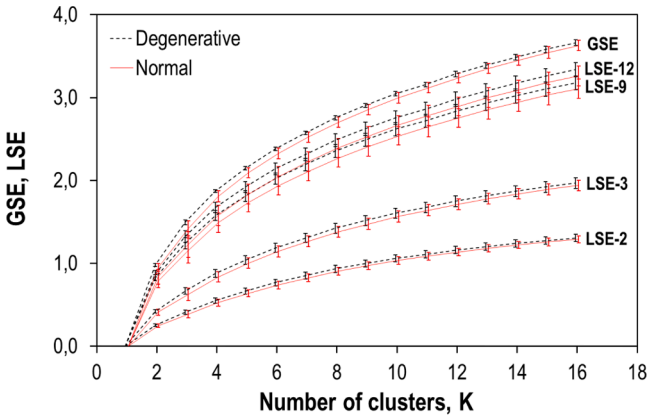

Fig. 5. Curves showing the relationship between entropy (GSE, LSE-2, LSE-3, LSE-9 and LSE-12) and the number of clusters, K. Continuous lines correspond to normal chords and dashed lines to degenerative samples.

calculated from a transformed histogram that considers internal variability instead of the contrast values given by micro-CT, which are subject to noise and sample variability –i.e., K-means normalizes by second order momentum.

This analysis was carried out by means of the MATLAB™ toolboxes for Image Processing, Statistics and Machine Learning as well as the R language for statistical computing and graphics.

2.4. Scanning electron and optical microscopy

Two randomly selected samples from each group were observed by SEM using a Carl Zeiss™ device model EVO MA15, equipped with detectors for secondary and retrodispersed electrons as well as X-rays (Oxford Instruments™). The chordal fragments, fixed in 3% glutaraldehyde, were dehydrated in graded acetone, dried by the critical point method, coated with gold, and observed with an Inspect S microscope. For conventional light microscopy, excised valves were fixed in 3% glutaraldehyde in PBS. The MCT were postfixed in 1% osmium tetroxide for 1 hour, dehydrated in graded acetone and propylene oxide, and embedded in Araldite. 1 µm sections were cut with a Leica Ultracut UCT, stained with 1% toluidine blue, and observed with a Zeiss III photomicroscope.

2.5. Statistics

The statistical analysis was aimed at evaluating the microstructural differences between normal (Group I: 14 MVs, 19 MCT) and degenerative MCT (Group II: 11 MV, 20 MCT) after micro-CT. Between one and two MCT were randomly obtained from each MV for this study. In this design, MVs are fully nested within groups (I and II) and the final data are slightly unbalanced (unequal sample sizes in each subgroup). The unequal variance nested ANOVA was chosen because of the (slightly) unbalanced design of the experiment. The significance threshold was set at 0.05. Calculations were carried out using the R software for statistical computing and graphics.

3. Results

Light microscopy and SEM were used to determine the morphology of normal and degenerative mitral valves [13]. The normal external appearance of the mitral valves (Group I) contrasts with the delicate fibroelastic degenerative mitral valves (Group II), in which the leaflets were very thin, friable and almost transparent.

3.1. Microstructural organization

Normal MCT are composed of a superficial layer of flat endothelial cells covering the underlying spongiosa layer protecting the organized collagen core. The boundaries between the shielding spongiosa and the smooth appearance dense core show no structural disruption, as proved by the micro-CT analysis. The central axis of each chord was obtained from image processing and then cross-sections normal to the central axis were selected. Fig. 1(a) shows a cross-section of one of the normal MCT of this study where the three structural layers can be identified. A longitudinal section of this chord is presented in Fig. 1(b), enabling the appreciation of how the collagen fibers maintain their individuality in the length of the MCT. These features are common for all normal MCT samples analyzed in this study and in agreement with the findings

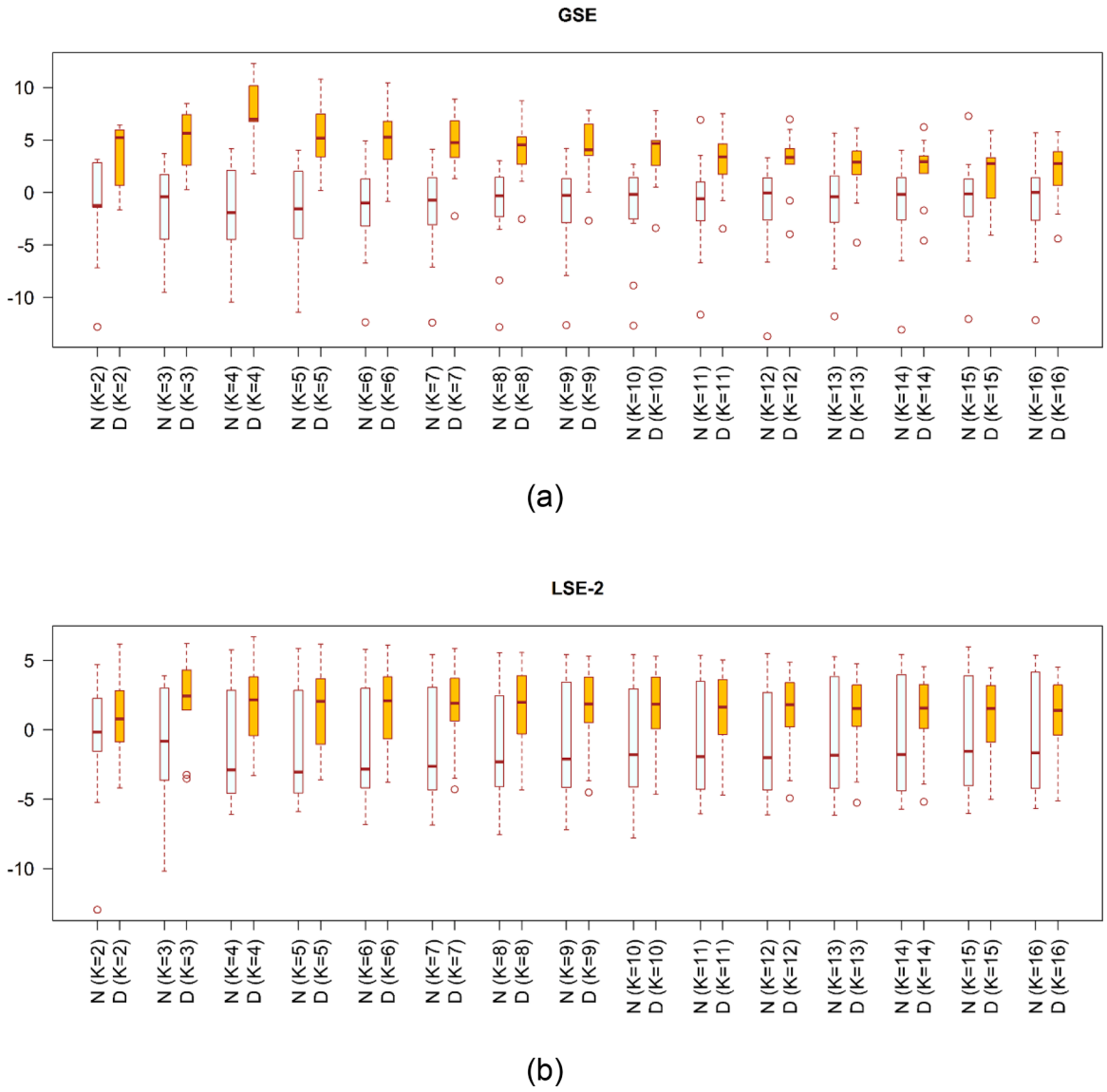

Fig. 6. Boxplots comparing normal and degenerative MCT as a function of K. (a) GSE, (b) LSE-2, (c) LSE-3, (d) LSE-9 and (e) LSE-12. 'N' and 'D' refer, respectively, to normal and degenerative MCT.

obtained through conventional light microscopy, Fig. 1(c), and SEM, Fig. 1(d). In both cases, normal MCT appears with an external layer of flat superficial endothelial (E) cells covering the underlying spongiosa (S) with the elastin fibers mostly limited to this fluffy layer. Collagen fibers are arranged in the normal wavy configuration, forming closely packed crimped bundles, where single fibers are rarely visible.

The most remarkable feature of degenerative MCT (Group II) consists in the grouping of the individual collagen fibers into coarse bundles, as shown in the micro-CT cross-section, Fig. 2(a), and demonstrated by the morphology of the longitudinal view, Fig. 2(b). The dense collagen core is arranged in bundles with a tendency to parallel configuration. The SEM micrograph in Fig. 2(c) shows that degenerative chordae are very loosely packed (individual fibers can be seen), forming an almost hairy appearance.

The scheme shown in Fig. 3 represents, in a simplified way, the organization of collagen in the longitudinal and transverse direction of the MCT.

The panel of micro-CT images in Fig. 4 allows the differences in structural organization of normal and degenerative MCT to be clearly discerned. The three images on the left correspond to normal chords while those on the right are samples from degenerative valves. In all of them, a magnified detail with a size of 100 × 100 μm has been obtained. All the images of normal chords characterized in this study have a fine texture, which contrasts with the coarse texture of the degenerative samples. Besides, degenerative chords show a coarse texture with greater variability. This fact is clearly seen in the three figures on the right.

3.3. *Analysis of micro-CT images through K-means clustering and shannon entropy*

Fig. 5 summarizes the results obtained from the K-means clustering procedure. It shows the curves that relate the entropic measures (GSE and LSE -2,3,9 and 12-) as a function of the number of clusters, K, for normal and degenerative chords (represented by solid and dashed lines, respectively). For each value of K, the mean value of the SE and the standard deviation of the group have been represented. Consistency was observed between the measures of texture since both entropic metrics increase with K. Entropy was systematically higher for degenerative chords (for each value of K), indicating a higher level of disorder in

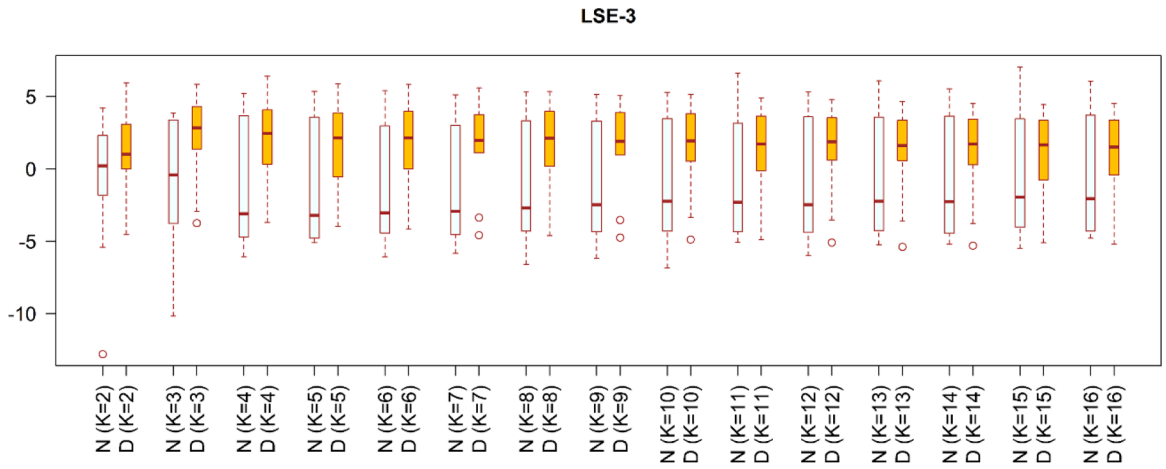

(c)

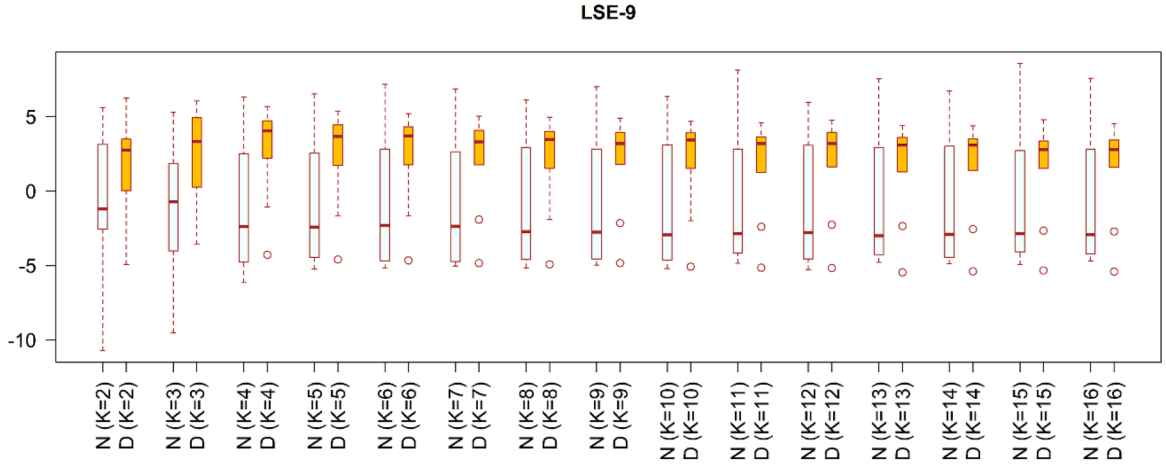

(d)

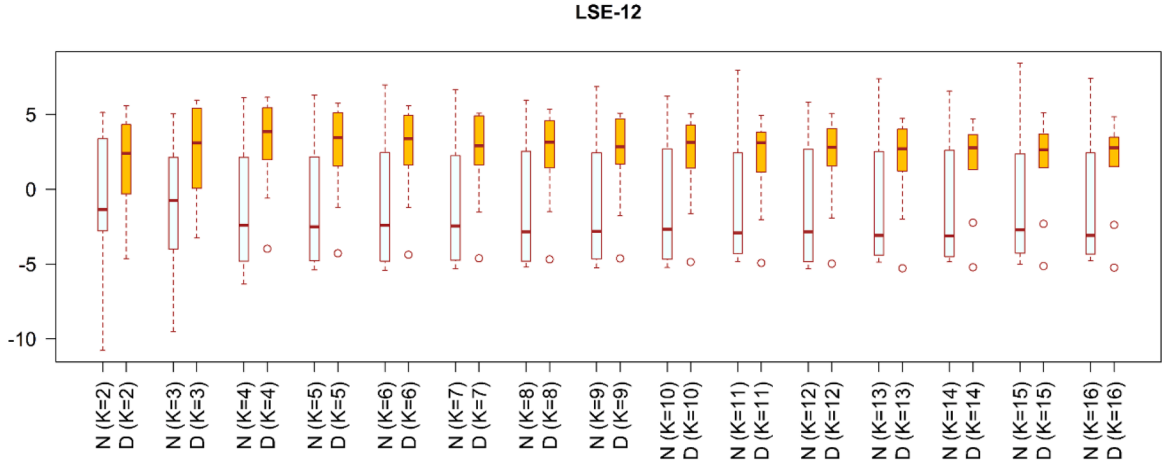

(e)

Fig. 6. (*continued*).

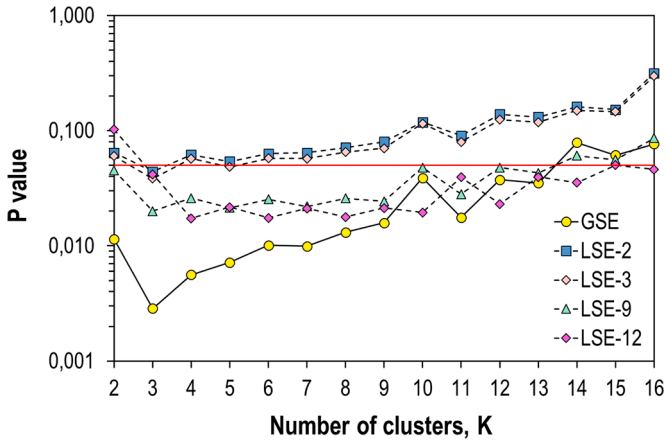

Fig. 7. Scatterplot showing the statistical significance (p-value) after comparing normal and degenerative MCT through a nested ANOVA test, as a function of the number of clusters, K.

normal MCT, in consistency with the less structured and more homogenous arrangement shown by the micro-CT images (see Fig. 4).

To display a more clarifying representation, boxplots are shown in Fig. 6 for each of the entropic measures (GSE and LSE 2, 3, 9 and 12) as a function of K, comparing normal and degenerative chords. To permit a reliable comparison, data were normalized subtracting, for each value of K, the joint mean of the corresponding normal and degenerative data and dividing, for each boxplot, by the standard error of the mean (i.e. the standard deviation of the sample divided by the square root of the number of observations). The large differences between normal and degenerative MCT are evident in GSE; moreover, the ability of LSE to separate between them increases steadily with the number of pixels (from 2 to 12).

The criterion adopted in this study for optimizing the number of clusters, K, is based on its ability to separate between normal and degenerative chords. For this reason, the p-values provided by the nested ANOVA conducted for the couple of boxplots corresponding to each value of K have been obtained and represented in Fig. 7 as a function of the number of clusters. The great ability of GSE as a separator is observed (the horizontal line corresponds to a level of significance of 0.05); thus, GSE with $3 \leq K \leq 7$ provides $p < 0.01$ and $p < 0.05$ for $2 \leq K \leq 13$; the optimum result corresponds to K=3, where $p = 2.86 \cdot 10^{-3}$ (in this case, the Jarque-Bera test was used to verify that the healthy and degenerative distributions match the normal distribution. In this case, $p = 0.513$ and 0.486 for the normal and degenerative MCT, respectively; therefore, there is no sufficient evidence to reject the null hypothesis). Moreover, the quality of LSE as a reliable separator improves by increasing the number of pixels and provides $p < 0.05$ for 9 and 12 pixels with $2 \leq K \leq 13$ and $3 \leq K \leq 16$, respectively.

4. Discussion

Mitral valve repair is the elective treatment for the majority of patients with degenerative disease. In most cases, valve reconstruction consists in the resection or replacement of the affected chords, together with annuloplasty. Nevertheless, the remaining chordae with normal appearance at surgery may well have already been affected by the degenerative process, as suggested by the significant rates of recurrence. In this study, we have selected the fibroelastic deficiency because it is the most common cause of degenerative mitral valve regurgitation due to ruptured chordae tendineae.

Micro-CT cross-section views of the degenerative marginal chords showed that the natural wavy configuration of the individual collagen fibrils was lost, being replaced by a layout of collagen bundles. The longitudinal views proved the straightened arrangement of these bundles of fibers, showing a tendency to line up with the axis of the chord. In our opinion, the formation of thickened bundles represents a microstructural feature that allows the degenerative disease to be identified.

An algorithmic procedure has been implemented to measure the texture of the images of the cross-sections of the MCT by means of the Shannon entropy (100 cross-sections for each chord). Previously, the K-means clustering method was applied on the histogram of grayscales of each image, with $2 \leq K \leq 16$. The results show that the differences in microstructural organization of normal and degenerative chords translate into statistically significant differences in terms of global Shannon entropy; thus, with $3 \leq K \leq 7$, $p < 0.01$ is obtained. The optimal result is reached with K=3 where $p = 2.86 \cdot 10^{-3}$. In addition, local Shannon entropy was obtained with 2, 3, 9 and 12 pixels, respectively. It was observed that the greater the number of pixels, the better the statistical significance and that with 9 and 12 pixels $p < 0.05$. The separation ability of local Shannon entropy decreases when the size of the window is 2 or 3 pixels. In these cases, sampling sometimes results in spurious sections that may correspond to noise or the edges of the collagen fibers. In contrast, for a size of the window of 9 and 12 pixels significance increases, which implies that collagen fibers are fully present in this range. It can be concluded that GSE is more efficient at separating both conditions at low quantization levels. Furthermore, differences in Shannon entropy are better captured by coarser scales, as shown by a decreasing level of statistical significance in finer levels of LSE. Since Shannon entropy is a contrast level distribution metric, it disregards information concerning internal or spatial organization. Through the usage of LSE, we show that differences in randomness between MCT conditions are scale-free, which implies that bundle changes can be explained from contrast at level of the fiber itself without considering the spatial arrangement. This implies LSE measures would be more inefficient at classifying tissue conditions if employed in a diagnosis system.

Our results indicate that normal and degenerative chords belong to different distributions according to their homogeneity as measured by a simple information metric as Shannon entropy. Hence, in contrast with previous supervised methods [31–34], we characterize structural differences in an unsupervised and parameter-free manner, which can be utilized for diagnosis. In previous studies fractal dimension has been used as an alternative method to classify tissue condition [35–39] in comparison, local Shannon entropy relies less in geometrical definitions and poses more a heterogeneity condition based on contrast levels (see Methods). Hence, our quantification captures structural changes across scales without assumptions on shape changes of bundles, thus, solely considering the overall pixel distribution. Both metrics can be used in combination to asset structural modifications [38], however, we show the local definition of Shannon entropy may be suitable enough in the case of MCT.

A final remark on the consequences of our study for the clinical diagnosis and identification of degenerative chords is mandatory. Intraoperative identification of the possible affected degenerative chordae tendineae is not possible with the current diagnostic tools, so prevention of recurrent mitral valve insufficiency is practically unmanageable. Unfortunately, micro-CT cannot be employed at surgery, at least under the current technological limits. Among the available techniques, Optical Coherence Tomography (OCT) represents a promising candidate as a diagnostic tool. OCT is an imaging technology that allows tissue samples to be visualized to a depth of millimeters, which is more than the thickness a mitral chord [40]. Moreover, it is a fast acquisition method that could provide real-time guidance on the internal structure of the MCT under intraoperative conditions. This technique has been successfully applied in previous studies by some of the authors of this paper. For instance, Real et al. have employed and validated OCT to examine aortic aneurysms [41] and mitral chordae tendineae [42] in human ex-vivo samples.

The most limiting drawback is that OCT only provides the birefringence pattern of the sample whose interpretation is far from

straightforward. This contrasts with the great advantage of micro-CT, namely, its ability to identify the constitutive microstructures of the tissue (the mitral chords in this case). Therefore, micro-CT and OCT are to be considered as complementary methods since the former provides the information necessary to validate the latter as a diagnostic technique. Such techniques may prove to be more successful than state-of-the-art methods like echocardiographic, ultrasound or scanning electrode microscope, which continue to rely on geometrical characteristics and expert opinion [43]. Our work shows that distribution differences between normal and pathological conditions of MCT, from an optical method as micro-CT, can be captured through a scalar metric as the Shannon entropy under different levels of quantization and scales. However, it must be noted that we do not provide a robust binary classifier based on this metric, but we present statistical differences between conditions that suggest that advanced machine learning methods could harness the power of bundle changes as captured by optical methods, in contrast with current acoustic approaches that are very data-intensive [44].

In conclusion, at this moment it seems possible to develop an intra-operative diagnostic technique that would reduce the number of re-currences associated with the current impossibility of identifying degenerative mitral chords.

Acknowledgements

This work is supported by the “Ministerio de Economía, Industria y Competitividad” (MINECO) and the “Instituto de Salud Carlos III” (ISCIII) of Spain, through projects INTRACARDIO (DTS17/00056) and CIBER-BBN (co-financed by FEDER funds) and IDIVAL under project DiCuTen (INNVAL16/02). The technical contributions from the members of the DICUTEN and the financial contribution from the IDIVAL are gratefully acknowledged.

The authors declare that they have no known competing financial interests or personal relationships that could have appeared to influence the work reported in this paper. This study was approved by the Ethical Committee of Clinical Research of Cantabria – IDIVAL (Acta 02/2018).

Supplementary materials

Supplementary material associated with this article can be found, in the online version, at doi:10.1016/j.medengphy.2022.103919.

References

[1] D’Arcy JL, Prendergast BD, Chambers JB, Ray SG, Bridgewater B. Valvular heart disease: the next cardiac epidemic. Heart 2011;97:91–3. https://doi.org/10.1136/hrt.2010.205096.
[2] Adams DH, Anyanwu AC, Rahmanian PB, Filsoufi F. Current concepts in mitral valve repair for degenerative disease. Heart Fail Rev 2006;11:241–57. https://doi.org/10.1007/s10741-006-0103-7.
[3] Casado JA, Diego S, Ferreño D, Ruiz E, Carrascal I, Méndez D, et al. Determination of the mechanical properties of normal and calcified human mitral chordae tendineae. J Mech Behav Biomed Mater 2012;13:1–13. https://doi.org/10.1016/j.jmbbm.2012.03.016.
[4] Lam J, Ranganathan N, Wigle E, Silver M. Morphology of the human mitral valve: I. Chordae tendineae: a new classification. Circulation 1970;41:449–58. https://doi.org/10.1161/01.CIR.41.3.449.
[5] Ranganathan N, Lam JH, Wigle ED, Silver MD. Morphology of the human mitral valve. Circulation 1970;41:459–67. https://doi.org/10.1161/01.CIR.41.3.459.
[6] Carpentier A, Chauvaud S, Fabiani J, Deloche A, Relland J, Lessana A, et al. Reconstructive surgery of mitral valve incompetency. J Thorac Cardiovasc Surg 1980;79:338–48.
[7] Carpentier A. Cardiac valve surgery-the “French correction. J Thorac Cardiovasc Surg 1983;86:323–37.
[8] Flameng W, Herijgers P, Bogaerts K. Recurrence of mitral valve regurgitation after mitral valve repair in degenerative valve disease. Circulation 2003;107:1609–13. https://doi.org/10.1161/01.CIR.0000058703.26715.9D.
[9] Mohty D, Orszulak TA, Schaff HV, Avierinos JF, Tajik JA, Enriquez-Sarano M. Very long-term survival and durability of mitral valve repair for mitral valve prolapse. Circulation 2001;104:1–7.
[10] Chikwe J, Adams DH. State of the Art: Degenerative Mitral Valve Disease. Hear Lung Circ 2009;18:319–29. https://doi.org/10.1016/j.hlc.2009.02.005.
[11] Anyanwu AC, Adams DH. Etiologic classification of degenerative mitral valve disease: Barlow’s disease and fibroelastic deficiency. Semin Thorac Cardiovasc Surg 2007;19:90–6. https://doi.org/10.1053/j.semtcvs.2007.04.002.
[12] van Wijngaarden AL, Kruithof BPT, Vinella T, Barge-Schaapveld DQCM, Ajmone Marsan N. Characterization of degenerative mitral valve disease: differences between fibroelastic deficiency and Barlow’s disease. J Cardiovasc Dev Dis 2021;8. https://doi.org/10.3390/jcdd8020023.
[13] Icardo JM, Colvee E, Revuelta JM. Structural analysis of chordae tendineae in degenerative disease of the mitral valve. Int J Cardiol 2013;167:1603–9. https://doi.org/10.1016/j.ijcard.2012.04.092.
[14] Ritchie J. The material properties of the chordae tendineae of the mitral valve: an in vitro investigations. Georgia Institute of Technology; 2004.
[15] Millington-Sanders C, Meir A, Lawrence L, Stolinski C. Structure of chordae tendineae in the left ventricle of the human heart. J Anat 1998;192:573–81.
[16] Revuelta JM, García-Rinaldi R, Gaite L, Val F, Garijo F. Generation of chordare tendineae with polytetrafluoroethylene stents. J Thorac Cardiovasc Surg 1989;97:98–103.
[17] Revuelta JM, Cagigas JC, Bernal JM, Val F, Rabasa JM, Lequerica MA. Partial Replacement mitral valve by homograft. An experimental study. J Thorac Cardiovasc Surg 1992;104:1274–9.
[18] Chen S, Sari CR, Gao H, Lei Y, Segers P, De Beule M, et al. Mechanical and morphometric study of mitral valve chordae tendineae and related papillary muscle. J Mech Behav Biomed Mater 2020;111:104011. https://doi.org/10.1016/j.jmbbm.2020.104011.
[19] Shannon CE. A mathematical theory of communication. Bell Syst Tech J 1948;27:623–56. 379–423.
[20] Prot V, Skallerud B, Sommer G, Holzapfel GA. On modelling and analysis of healthy and pathological human mitral valves: two case studies. J Mech Behav Biomed Mater 2010;3:167–77. https://doi.org/10.1016/j.jmbbm.2009.05.004.
[21] Gunning GM, Murphy BP. Characterisation of the fatigue life, dynamic creep and modes of damage accumulation within mitral valve chordae tendineae. Acta Biomater 2015;24:193–200. https://doi.org/10.1016/j.actbio.2015.06.015.
[22] Grbic S, Ionasec R, Vitanovski D, Voigt I, Wang Y, Georgescu Bogdan, et al. Complete valvular heart apparatus model from 4D cardiac CT. Med Image Anal 2012;16:1003–14.
[23] Wu Y, Zhou Y, Saveriades G, Agaian S, Noonan JP, Natarajan P. Local Shannon entropy measure with statistical tests for image randomness. Inf Sci (Ny) 2013;222:323–42. https://doi.org/10.1016/j.ins.2012.07.049.
[24] Shapiro L, Stockman G. Computer vision. Pearson; 2000.
[25] Biomedical texture analysis. In: Depeursinge A, Al-Kadi OS, Mitchell JR, editors. Fundamentals, tools and challenges; 2017.
[26] Knops ZF, Maintz JBA, Viergevera MA, Pluim JPW. Normalized mutual information based registration using k-means clustering and shading correction. Med Image Anal 2006;10:432–9.
[27] Niemeijer M, Abràmoff MD, Ginneken B. Image structure clustering for image quality verification of color retina images in diabetic retinopathy screening. Med Image Anal 2006;10:888–98.
[28] Palubinskas G. K-means clustering algorithm using entropy. In: Proc. SPIE 3500, Image Signal Process. Remote Sens. IV; 1998. p. 63–71. https://doi.org/10.1117/12.331894.
[29] McLean GF. Vector quantization for texture classification. IEEE Trans Syst Man Cybern 1993;23:637–49. https://doi.org/10.1109/21.256539.
[30] Wachinger C, Navab N. Entropy and Laplacian images: Structural representations for multi-modal registration. Med Image Anal 2012;16:1–17.
[31] Scott-Jupp W, Barneti NL, Gallagher PJ, Monro JL, Ross JK. Ultrastructural changes in spontaneous rupture of mitral chordae tendineae. J Pathol 1981;133:185–201.
[32] Uğuz H, Arslan A, Türkoğlu I. A biomedical system based on hidden Markov model for diagnosis of the heart valve diseases. Pattern Recognit Lett 2007;28:395–404. https://doi.org/10.1016/j.patrec.2006.08.009.
[33] Anbarasi A, Ravi S, Vaishnavi J, Matla SVSB. Computer aided decision support system for mitral valve diagnosis and classification using depthwise separable convolution neural network. Multimed Tools Appl 2021;80:21409–24. https://doi.org/10.1007/s11042-021-10770-x.
[34] Fernando T, Gammulle H, Denman S, Sridharan S, Fookes C. Deep learning for medical anomaly detection a survey. ACM Comput Surv 2022;54:1–28. https://doi.org/10.1145/3464423.
[35] Smith TG, Lange GD, Marks WB. Fractal methods and results in cellular morphology - dimensions, lacunarity and multifractals. J Neurosci Methods 1996;69:123–36. https://doi.org/10.1016/S0165-0270(96)00080-5.
[36] Balocchi R. Fractal dimension: from geometry to physiology. adv. methods biomed. signal Process. John Wiley & Sons, Ltd; 2011. p. 327–46. https://doi.org/10.1002/9781118007747.ch13.
[37] Yalta K, Ozturk S, Yetkin E. Golden Ratio and the heart: a review of divine aesthetics. Int J Cardiol 2016;214:107–12. https://doi.org/10.1016/j.ijcard.2016.03.166.
[38] Kolossváry M, Kellermayer M, Merkely B, Maurovich-Horvat P. Cardiac computed tomography radiomics. J Thorac Imaging 2018;33:26–34. https://doi.org/10.1097/RTI.0000000000000268.
[39] Deorsola L, Bellone A. Interventional Cardiology Golden ratio and fractals in mitral valve geometry : potential implications for valve imaging assessment. Interv Cardiol 2021;13:332–40.
[40] Baghaie A, Yu Z, D’Souza RM. Involuntary eye motion correction in retinal optical coherence tomography: hardware or software solution? Med Image Anal 2017;37:129–45.

[41] Real E, Val-Bernal JF, Revuelta JM, Pontón A, Calvo M, Mayorga M, et al. Hessian analysis for the delineation of amorphous anomalies in optical coherence tomography images of the aortic wall. Biomed Opt Express 2016;7:1415–29. https://doi.org/10.1364/BOE.7.001415.

[42] Real E, Revuelta JM, González-Vargas N, Pontón A, Calvo M, López-Higuera JM, et al. Collagen birefringence assessment in heart chordae tendineae through PS-OCT. In: Opt. coherence tomogr. coherence domain opt. methods biomed. XXI, Photonics West BiOS; 2017.

[43] Levine RA, Hagége AA, Judge DP, Padala M, Dal-Bianco JP, Aikawa E, et al. Mitral valve disease–morphology and mechanisms. Nat Rev Cardiol 2015;12:689–710. https://doi.org/10.1038/nrcardio.2015.161.

[44] Penso M, Pepi M, Mantegazza V, Cefalù C, Muratori M, Fusini L, et al. Machine learning prediction models for mitral valve repairability and mitral regurgitation recurrence in patients undergoing surgical mitral valve repair. Bioeng 2021;8. https://doi.org/10.3390/bioengineering8090117.